

On the calculation of wave attenuation along rough strings using individual and effective fields

Sebastian Rupprecht, Luke G. Bennetts, Malte A. Peter

Angaben zur Veröffentlichung / Publication details:

Rupprecht, Sebastian, Luke G. Bennetts, and Malte A. Peter. 2019. "On the calculation of wave attenuation along rough strings using individual and effective fields." Wave Motion 85: 57–66. <https://doi.org/10.1016/j.wavemoti.2018.10.007>.

Nutzungsbedingungen / Terms of use:

licgercopyright

Dieses Dokument wird unter folgenden Bedingungen zur Verfügung gestellt: / This document is made available under the following conditions:

Deutsches Urheberrecht

Weitere Informationen finden Sie unter: / For more information see:

<https://www.uni-augsburg.de/de/organisation/bibliothek/publizieren-zitieren-archivieren/publizieren>



On the calculation of wave attenuation along rough strings using individual and effective fields

Sebastian Rupprecht^a, Luke G. Bennetts^b, Malte A. Peter^{a,c}

^a*Institute of Mathematics, University of Augsburg, 86135 Augsburg, Germany*

^b*School of Mathematical Sciences, University of Adelaide, Adelaide 5005, Australia*

^c*Augsburg Centre for Innovative Technologies, University of Augsburg, 86135 Augsburg, Germany*

Abstract

The ability to analyse attenuation rates of individual wave fields along rough media using the effective wave field is investigated for the problem of a string with continuous, randomly varying properties. A clustering method is developed to approximate the continuous problem as a discrete problem, which provides insights into the relationship between the effective and individual wave fields. It is found that as scattering strength increases the attenuation rate of the effective wave field experiences a rapid transition from being orders of magnitude greater than the attenuation rate of its constituent individual wave fields to being almost identical to them.

Keywords: Wave attenuation, continuous scattering, discrete scattering, localisation, effective wave field

1. Introduction

Due to the wave localisation phenomenon (cf. Sheng, 2006, e.g.), a monochromatic incident wave train will typically attenuate exponentially along a rough (randomly disordered) medium, without the influence of any dissipative mechanism. Effective media theory is an appealing way to approach the problem of calculating the exponential attenuation rate — commonly referred to as the attenuation coefficient — as a function of the incident wave properties (frequency) and the properties of the given medium, including the statistical properties of the roughness. Effective media theory uses the effective wave field, which is the mean wave field with respect to an ensemble of individual wave fields obtained for single roughness realisations. Associated analytical methods for effective media theory provide insights into the attenuation process, and circumvent the need to compute individual wave fields for different realisations of the disorder.

Email addresses: sebastian.rupprecht@math.uni-augsburg.de (Sebastian Rupprecht), luke.bennetts@adelaide.edu.au (Luke G. Bennetts), malte.peter@math.uni-augsburg.de (Malte A. Peter)

For wave propagation along one-dimensional, continuously varying, rough media, it has been shown that the attenuation coefficient found using effective media theory often significantly overestimates the attenuation rate of the individual wave fields. In particular, Bennetts et al. (2015) investigated ocean wave propagation over a continuously varying, rough seabed in intermediate water depth, and found that individual wave fields generally do not attenuate, whereas effective wave fields experience significant attenuation. Wu (1982) and Rupprecht et al. (2017) made similar findings for seismic waves and flexural waves, respectively.

The left-hand panel of Fig. 1 shows the attenuation coefficients (later denoted \mathcal{C}) of individual and effective wave fields for a rough string with continuously varying density (the prototype problem used for this study), as functions of the roughness correlation length (later denoted l_G). The attenuation coefficient is non-dimensionalised with respect to the mean wavenumber, \bar{k} , and scaled using the roughness amplitude squared, ν^2 , and the correlation length is non-dimensionalised using the mean wavenumber.

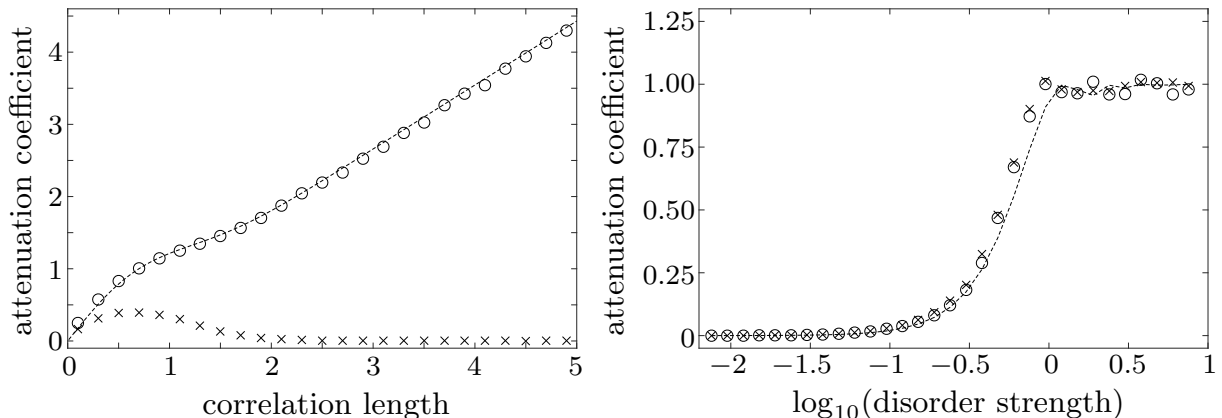


Figure 1: Left-hand panel: non-dimensional, scaled attenuation coefficient (later denoted $(\mathcal{C}/\bar{k})/\nu^2$) as a function of non-dimensional correlation length (later $\bar{k}l_G$) for a continuously varying string (with roughness amplitude $\nu = 1.0 \times 10^{-2}$). Numerical results for individual (\times) and effective (\circ) wave fields, with results given by a multiple-scale method shown for comparison (dashed line). Right-hand panel: non-dimensional, scaled attenuation coefficient $((\mathcal{C}/k)/\Gamma_{\text{BK}})$ as a function of scaled positional disorder $(\varepsilon k d/\pi)$ for discrete beaded-string problem (with scattering strength $i\eta = 0.2$). Numerical results for individual (\times) and effective (\circ) wave fields, with results given by CPA shown for comparison (dashed line).

The attenuation coefficient for the individual wave fields are calculated numerically using a random sampling method, and the attenuation coefficient for the effective wave field is calculated both numerically and analytically (using a multiple-scale approach). The results shown are cognate to those given by Bennetts et al. (2015) and Rupprecht et al. (2017) (who provide detailed descriptions of analogous multiple-scale approaches to the one used for the varying string). In particular, the attenuation coefficient for the effective wave field grows for increasing correlation length, which is merely a statistical effect caused by wave cancellation in the averaging process, whereas the attenuation coefficient for the individual wave fields is approximately zero for (non-dimensional) correlation lengths greater than two.

The situation appears to be different for problems involving disordered discrete scatterers, which have received significant attention since the late 1950s due to the seminal work of Anderson (1958), who proposed localisation of electrons in disordered systems for sufficiently large randomness. An example from classical physics, for which effective media theory works well, is linear wave propagation along a string with randomly positioned beads attached. More precisely, identical point masses are distributed along an elastic string, with their positions randomly perturbed from a periodic arrangement. The perturbed periodic problem has been studied extensively over the last decade and analytical theories have been adopted to describe the effective wave field, e.g. a quasi-crystalline assumption considering perturbations from an underlying periodic setting (Parnell and Abrahams, 2008) and the coherent potential approximation based on a closure assumption (Maurel et al., 2010). Romack and Weaver (1990) used a Monte Carlo method for vibrations in beaded strings to study effective waves in one-dimensional random media composed of uncorrelated point scatterers with exponentially distributed scatterer spacings. Maurel and Martin (2013) showed that localised modes appear in disordered media of finite size (using perturbation theory) and also studied compositional disorder. Martin (2014) used perturbation theory to study finite beaded strings with perturbations of the masses from their periodic structure by a small distance. For the cognate problem of rows of discrete scatterers, Bennetts and Peter (2013) showed that individual and effective wave fields have almost identical attenuation coefficients.

In the case of large positional disorder of the discrete scatterers, an attenuation coefficient related to the individual wave fields can be derived in a simple way using the method proposed by Berry and Klein (1997) for light propagation through a stack of transparent plates. More precisely, if it is assumed that wave interactions between adjacent (identical) scatterers range over all phases, which requires that $\varepsilon k d / \pi \geq 1$, where $\varepsilon \in [0, 1)$ is the non-dimensional disorder strength ($\varepsilon = 0$ denoting unperturbed), k is the wavenumber and d is the spacing of the underlying periodic structure, then the attenuation rate is $\Gamma_{\text{BK}} = \ln |\tau|$, where τ is the transmission coefficient for a single scatterer, which is related to its (real-valued) scattering strength $i\eta$ by $\tau = 1/(1 - \eta)$. Hence, we refer to $\varepsilon k d / \pi = 1$ as the positional-disorder threshold.

The right-hand panel of Fig. 1 shows individual and effective attenuation coefficients for the discrete problem of positionally perturbed beads along an elastic string, as a function of scaled, non-dimensional positional disorder ($\varepsilon k d / \pi$). The attenuation coefficient is normalised using the Berry–Klein limit (BK limit, Γ_{BK}). Analytical results obtained with a coherent potential approximation (CPA), as derived by Maurel et al. (2010), are shown for comparison. The individual and effective attenuation coefficients agree well for the whole range of positional disorder and they agree with the BK limit beyond the positional-disorder threshold. In particular, the attenuation rate for the effective wave field is almost identical to that of the individual wave fields for the range of disorder strengths considered.

Thus, sometimes the effective wave field has an attenuation rate that is representative of attenuation rates of individual wave fields (i.e. for the discrete problem) and sometimes its attenuation rate is much larger than the individual wave fields (i.e. for the continuous problem). This paper investigates this phenomenon for the problem of attenuation of linear

waves along strings with discrete or continuous random variations, which can be viewed as model problems for waves in more complicated media but containing the relevant physics. It is shown that the attenuation rates of effective and individual wave fields transition from being significantly different to almost identical.

The paper is organised as follows: In §2, the problem formulation for wave propagation along a one-dimensional string with continuously varying density profile is defined, and a numerical solution method is introduced. Further, the different attenuation coefficients are defined precisely and their computation is discussed. In §3, the continuous problem is approximated by a discrete problem using a clustering approach, thus facilitating investigation of the transition between the two behaviours. In §4, the main result of the paper is given, which is the characterisation of the relation between individual and effective waves along a rough string. A summary of the results is given in §5.

2. Preliminaries

2.1. Problem formulation and solution method

Consider an infinitely long, one-dimensional, linearly elastic, stretched string, where the horizontal coordinate x denotes position along the undisturbed string. The string undergoes small amplitude, time-harmonic displacements at a prescribed angular frequency ω , so that the displacement can be written $\text{Re} \{u(x) e^{-i\omega t}\}$, where t denotes time. The spatial component of the displacement, $u = u(x)$, satisfies the Helmholtz equation,

$$u'' + k^2 u = 0 \quad \text{for} \quad x \in (-\infty, \infty), \quad (1)$$

where the wavenumber $k = k(x)$ is rough, i.e. has a randomly fluctuating profile, produced by underlying variations in the properties of the string, e.g. in its density. In this setting,

$$k(x) = \omega \sqrt{\frac{\mu(x)}{T}}, \quad (2)$$

where μ is the mass per unit length and T is the tension force.

Let the rough wavenumber profile, k , be a random function with an associated expectation \mathbf{E} (with respect to space). It has the form

$$k(x) = \bar{k} \left(1 + \nu \kappa(x)\right) \quad \text{with} \quad \kappa = \mathcal{O}(1), \quad (3)$$

where $\bar{k} = \mathbf{E}[k]$ is a prescribed mean, and $\bar{k} \nu = \sqrt{\mathbf{E}[k^2]}$ is a prescribed root-mean-square amplitude. Wavenumber roughness is produced by the zero-mean random function κ , with $\sqrt{\mathbf{E}[\kappa^2]} = 1$. The function κ is assumed to be stationary and ergodic, so that $\bar{\kappa}$ is the spatial mean of the rough wavenumber, and ν is the root-mean square amplitude with respect to space, and hence referred to as the (non-dimensional) roughness amplitude. For the sake of definiteness, the random functions considered satisfy the Gaussian autocorrelation condition

$$\mathbf{E}[\kappa(x)\kappa(x - \xi)] = e^{-\xi^2/l_G^2}, \quad (4)$$

where l_G is the correlation length.

Following Shinozuka (1971), individual realisations of the random function are generated via

$$\kappa(x) = \sqrt{\frac{2}{H}} \sum_{h=1}^H \cos(r_h x + \varphi_h) \quad \text{for} \quad H \gg 1, \quad (5)$$

where the frequencies r_h ($h = 1, \dots, H$) are random variables, independently chosen from a Gaussian distribution with zero mean and standard deviation of $\sqrt{2}/l_G$, and the phases φ_h ($h = 1, \dots, H$) are independently selected from a uniform distribution over the interval $[0, 2\pi)$. These satisfy the autocorrelation condition (4) in the limit $H \rightarrow \infty$. In practice, $H = 400$ terms are used in the random process (5).

For numerical computations, let the variations extend over a long, finite interval $x \in (0, L)$, where $L \gg 2\pi/\bar{k}$, and be constant in the surrounding intervals $(-\infty, 0)$ and (L, ∞) . The rough wavenumber profile is approximated by the so-called step approximation, consisting of a piece-wise constant function on $M \gg 1$ sub-intervals over $x \in (0, L)$, where the value of the constant wavenumber in each sub-interval, k_m ($m = 1, \dots, M$), is set to be equal to the value of the corresponding continuous wavenumber profile at the sub-interval mid-point. The surrounding semi-infinite intervals, $(-\infty, 0)$ and (L, ∞) , are referred to as the 0-th and $(M + 1)$ -th sub-intervals, respectively, and the wavenumbers, k_0 and k_{M+1} , are set as the (constant) wavenumbers in the respective intervals. Fig. 2 shows an example realisation of a continuous wavenumber profile for roughness amplitude $\nu = 0.1$, and the corresponding piece-wise constant approximation of the profile, where each correlation length is divided into four sub-intervals, which provides sufficient computational accuracy.

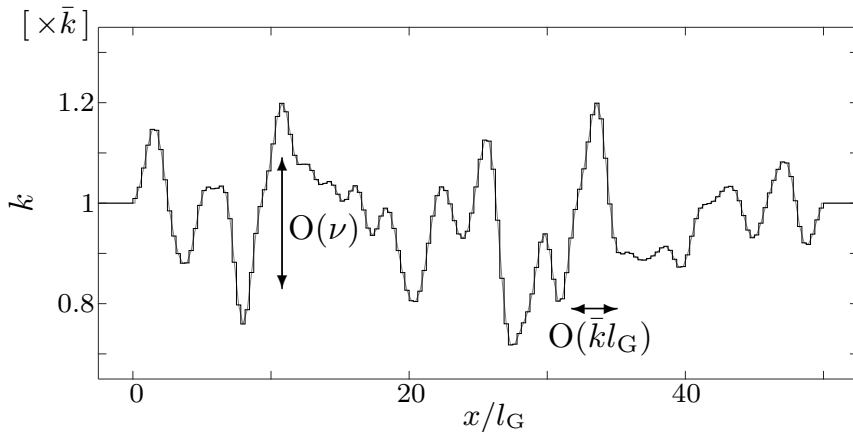


Figure 2: Example realisation of continuous roughness profile (grey curve) and corresponding step approximation with four sub-intervals per correlation length (black), for roughness amplitude $\nu = 0.1$ (adapted from Fig. 1 of Rupprecht et al., 2017).

In the m -th sub-interval, the wave field can be expressed as

$$u_m(x) = a_m e^{ik_m x} + b_m e^{-ik_m x}, \quad (6)$$

where a_m and b_m are amplitudes of right- and left-travelling waves, respectively. Motion is forced by a unit-amplitude incident wave propagating in the positive x -direction from $x \rightarrow -\infty$, which is set via $a_0 = 1$ and $b_{M+1} = 0$. Wave fields in adjacent sub-intervals are coupled via continuity conditions of displacement, u , and displacement slope, u' . The continuity conditions are applied at the jumps between the finite sub-intervals within the rough interval, and the jumps at the ends of the rough interval and the surrounding semi-infinite intervals ($x = 0, L$). The continuity conditions between the rough and semi-infinite intervals are ensured numerically by considering only profile realisations with sufficiently small steps at the respective interfaces. A modified version of the iterative algorithm developed by Bennetts and Squire (2009) is used to calculate the amplitudes a_m ($m = 1, \dots, M + 1$) and b_m ($m = 0, \dots, M$) for a given roughness realisation.

Over long distances L , roughness amplitudes larger than $\nu \approx 0.2$ generate negative wavenumbers in (3), which are viewed as being unphysical due to the assumed relationship with the material parameter in (2), i.e. they correspond to complex-valued densities μ . Therefore, a numerical cutoff scheme is applied, in which wavenumbers $k_m < 0.01$ are set to $k_m = 0.01$. This permits roughness amplitudes $\nu > 0.2$ to be investigated, unlike the previous cognate studies by Bennetts et al. (2015) and Rupprecht et al. (2017). The cutoff means the autocorrelation (4) is no longer satisfied exactly as $H \rightarrow \infty$, but this does not influence the key findings of the investigation.

2.2. Attenuation coefficients

The attenuation coefficient, \mathcal{C} , of an individual wave field, i.e. the exponential attenuation rate, is found by applying the ansatz

$$|u(x)| \propto e^{-\mathcal{C}x} \quad \text{for} \quad x \in (0, L), \quad (7)$$

using a least-squares minimisation routine. A representative attenuation coefficient, \mathcal{C}_{ind} , for wave fields produced by given statistical properties of the roughness (roughness amplitude, ν , and correlation length, l_G) is then calculated as

$$\mathcal{C}_{\text{ind}} = \langle \mathcal{C} \rangle, \quad (8)$$

where $\langle \cdot \rangle$ denotes the ensemble average of the included quantity, i.e. its mean with respect to a large number of randomly generated realisations of the rough wavenumber. An ensemble size of 1500 is used for calculations.

Similarly, the effective wave field for given statistical properties of the roughness, u_{eff} , is calculated numerically as the ensemble average

$$u_{\text{eff}} = \langle u \rangle. \quad (9)$$

The attenuation coefficient for the effective field, \mathcal{C}_{eff} , is then calculated via

$$|u_{\text{eff}}(x)| \propto e^{-\mathcal{C}_{\text{eff}}x} \quad \text{for} \quad x \in (0, L). \quad (10)$$

Ansatz (10) accurately captures the modulus of the effective wave field, up to numerical discrepancies, whereas ansatz (7) captures the mean attenuation of the individual wave

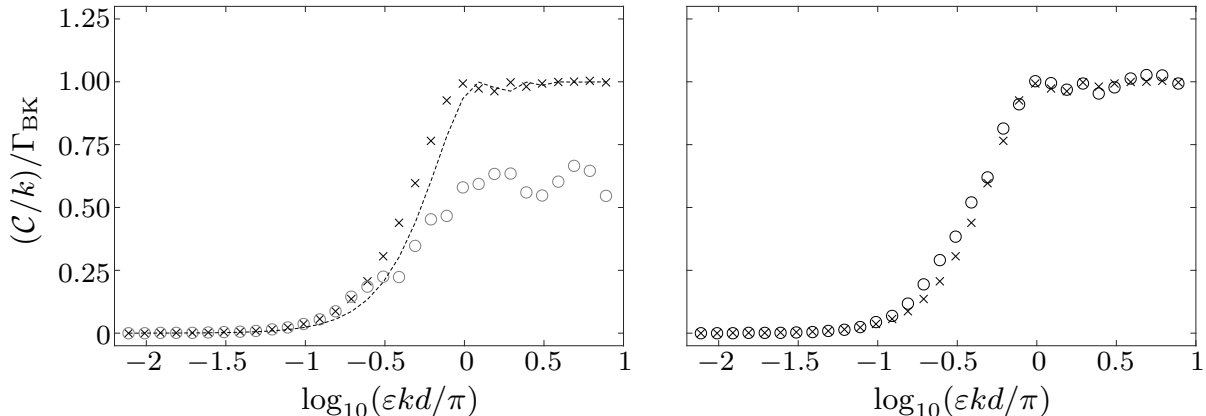


Figure 3: Left-hand panel: As in the right-hand panel of Fig. 1 but for scattering strength $i\eta = 0.6$. Right-hand panel: As in the left-hand panel but with individual (\times) and effective (\circ) attenuation coefficients calculated using percentile approach, and with CPA results omitted.

field only, neglecting fluctuations in the wave field that result from its dependence on the associated random wavenumber profile. For the numerical results presented in §§ 3–4, an interval length approximately 400 times the correlation length, $L \approx 400 \times l_G$, was found to be sufficiently large to capture wave attenuation accurately.

2.3. Calculation of effective attenuation coefficient

The left-hand panel of Fig. 3 is similar to the right-hand panel of Fig. 1, but for the larger scattering strength $i\eta = 0.6$. It shows individual and effective attenuation coefficients, \mathcal{C}_{ind} and \mathcal{C}_{eff} , respectively, calculated using the method described in § 2.2, for the relatively simple, beaded-string problem described in § 1, and we refer to the notation introduced there. The attenuation coefficients are scaled by the BK limit, Γ_{BK} , which is available for this discrete problem, and shown as functions of scaled positional disorder, and the CPA derived by Maurel et al. (2010) is overlaid for comparison.

The individual attenuation coefficient is approximately zero for

$$\log_{10}(\varepsilon k d / \pi) < -1,$$

and then monotonically increases to the BK limit at $\log_{10}(\varepsilon k d / \pi) = 0$, as expected. The CPA predicts the same behaviour, with only slightly smaller values in the increasing interval. However, the effective attenuation coefficient is consistent with the individual attenuation coefficient and CPA only up to $\log_{10}(\varepsilon k d / \pi) \approx -0.5$. For larger disorder strengths, the effective attenuation coefficient is smaller than individual attenuation coefficient, and for $\log_{10}(\varepsilon k d / \pi) > 0$ it is 30–40% smaller, hence also 30–40% smaller than the BK limit.

The unexpected behaviour in the effective attenuation coefficient contrasts with the results shown in the right-hand panel of Fig. 1, in which it agrees with the the individual attenuation coefficients and CPA over the full range positional disorders considered. The agreement could potentially be improved by extending the length L of the interval, but, for

practical purposes where the interval is short enough that calculations are not prohibitively time consuming, there exists a scattering strength above which the effective attenuation coefficient does not reach the BK limit. For the chosen length, $L \approx 400 \times l_G$, the effective attenuation coefficient does not reach the BK limit for scattering strengths $i\eta > 0.25$, and cognate behaviour occurs in the varying string problem.

A straightforward method to overcome the inconsistency in the numerical calculations is to form the effective wave field from an ensemble containing only individual fields with attenuation coefficients within the 25th–75th percentiles of all individual attenuation coefficients, thus eliminating the handful of individual wave fields in the ensemble that attenuate much more slowly than the other wave fields, which dominate the effective wave field at large propagation distances. The total ensemble size is increased to 3000, so that the effective field is still formed from 1500 individual fields. The right-hand panel of Fig. 3 shows that this method produces an effective attenuation coefficient that agrees with the individual attenuation coefficient, and, in particular, reaches the BK limit for large disorder. The modified method will be used to calculate all effective fields for the remainder of this study.

3. Clustering: discrete approximation of continuous problem

Each realisation of the wavenumber profile is clustered into humps, where a hump is defined as the profile between successive local minima, with respect to the step approximation. (Defining humps in terms of local minima is arbitrary, and local maxima or similar could equally be used.) Fig. 4 illustrates clustering of a wavenumber profile into humps for a section of the profile shown in Fig. 2.

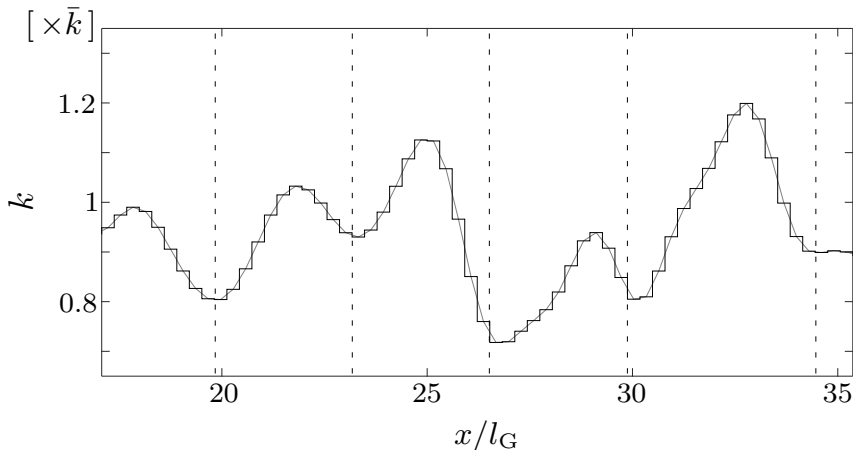


Figure 4: Example of clustering scheme applied to step approximation (black curve) of a rough wavenumber profile (grey), divided into clustered hump intervals (black broken vertical lines).

The complex-valued reflection coefficient for each hump, $R_{\text{hmp}} \in \mathbb{C}$, is calculated by applying the iterative algorithm discussed in § 2.1 to the steps in the interval occupied by the hump, i.e., having applied the method to the hump, it is given by b_0 in (6). The left-hand panel of Fig. 5 shows the mean clustered reflection coefficient modulus, $\langle |R_{\text{hmp}}| \rangle_{\text{hmp}}$,

where $\langle \cdot \rangle_{\text{hmp}}$ denotes the ensemble average with respect to humps in a profile of length $L = 40000 \times l_G$, giving ~ 15000 humps, as a function of non-dimensional correlation length, $\bar{k} l_G$, for roughness amplitude $\nu = 0.1$. The mean reflection increases with increasing correlation length up to $\bar{k} l_G \approx 0.7$, i.e. a wavelength ~ 3 times the mean hump length, after which it decreases, slowly tending to zero as the correlation length becomes large.

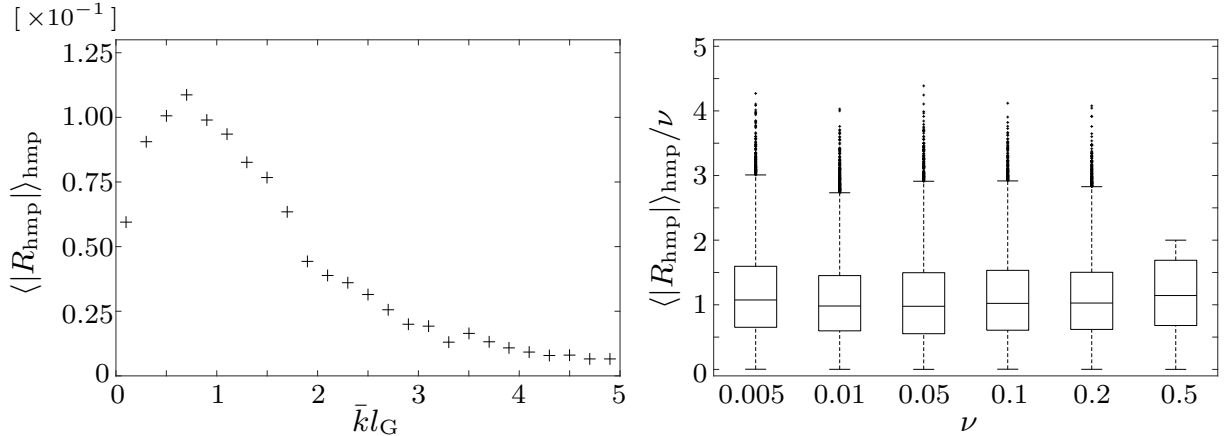


Figure 5: Left-hand panel: Scaled mean clustered reflection coefficient modulus as a function of correlation length, for roughness amplitude $\nu = 0.1$. Right-hand panel: Box-and-whisker plot of scaled clustered reflection coefficient moduli for different roughness amplitudes, for non-dimensional correlation length $\bar{k} l_G = 0.7$. The boxes indicate the intervals containing the central 50% of the clustered reflection coefficient moduli (25% to 75% percentiles), and the horizontal lines within them denote the median values (50% percentiles). The whiskers indicate the remaining sampled data lying in the range of 1.5 times the height of the central box next to the percentiles. Data points outside this range are considered to be outliers and are shown as crosses.

The right-hand panel of Fig. 5 shows box-and-whisker plots of the reflection modulus, scaled by the roughness amplitude, ν , as a function of the roughness amplitude, and for $\bar{k} l_G = 0.7$. The reflection coefficient appears to scale with the roughness amplitude. In particular, the medians of the scaled reflection coefficients are similar, with no evidence of a trend. The overall distributions are similar for $\nu = 0.01$ – 0.2 , but differ for $\nu = 0.5$, with, in particular, no outliers appearing for $\nu = 0.5$ and the upper whisker being relatively small due to the numerical cutoff scheme reducing the range of hump amplitudes. However, the interquartile range (the box) is consistent with the smaller roughness amplitudes.

Fig. 6 shows the distribution of the reflection coefficient phases, $\arg(R_{\text{hmp}})$, for the non-dimensional correlation lengths $\bar{k} l_G = 0.7$ (left-hand panel) and $\bar{k} l_G = 2.5$ (right). The distributions are overlaid by a non-parametric probability density function, which is fitted using a kernel density estimator (Silverman, 1986). For the shorter correlation length, $\bar{k} l_G = 0.7$, the distribution is approximately bell-shaped, with its mode just above 1.1π , and slightly skewed towards phase changes between 0.3π and 0.8π . For $\bar{k} l_G = 2.5$, the mode is close to $3\pi/2$, and the distribution is broader than for $\bar{k} l_G = 0.7$, covering all phases.

The wavenumber profile clustering is used to form an approximate mapping of the varying

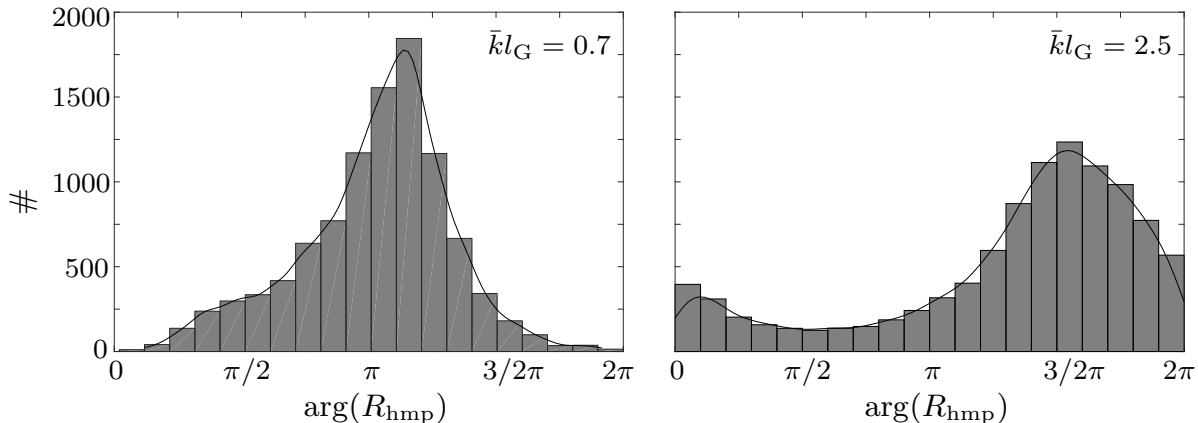


Figure 6: Distributions of reflection coefficient phases for roughness amplitude $\nu = 0.1$ and non-dimensional correlation length $\bar{k}l_G = 0.7$ (left-hand panel) and $\bar{k}l_G = 2.5$ (right). Fitted kernel distributions are overlaid (black curves).

string problem to a discrete problem, allowing it to be analysed in analogous fashion to the discrete problem of § 1 and § 2.3, with the constant wavenumber $k \equiv \bar{k}$ for consistency with the continuous problem. In analogy to the discrete problem, a scattering strength equivalent to the mean reflection coefficient is calculated as

$$i\eta = \frac{i \langle \langle |R_{\text{hmp}}| \rangle \rangle}{1 + \langle \langle |R_{\text{hmp}}| \rangle \rangle}, \quad (11)$$

where $\langle \langle \cdot \rangle \rangle$ denotes the ensemble average with respect to realisations and humps in the realisations. In practice, the scattering strength is increased by increasing the roughness amplitude, noting that the value of the scattering strength also depends on the correlation length, as shown in Fig. 5. The kernel functions are used to approximate the phase changes, which are induced by the different scatterer separations in the discrete problem, and the phase changes and scattering strengths are considered to be uncorrelated.

Fig. 7 shows individual attenuation coefficients, scaled by the BK limit, as functions of scattering strength, for the continuously varying string problem (outlined in § 2.1), and its discrete analogue formed from the clustering method. In all cases, the scaled attenuation coefficient for the discrete problem is insensitive to the scattering strength, noting that the BK limit scaling means the values shown do not tend to zero as the scattering strength tends to zero. For the smallest correlation length, $\bar{k}l_G = 0.7$, the scaled attenuation coefficient for the continuous problem closely matches the attenuation coefficient found by clustering, but with some indication of a trend to decrease as the scattering strength increases, particularly for scattering strengths greater than $i\eta \approx 0.18$. This behaviour is presumably due to the reflection coefficient, R_{hmp} , covering a greater range of values as the roughness amplitude/scattering strength increases. The trend becomes more pronounced for the intermediate correlation lengths, $\bar{k}l_G = 0.9$ and 1.1 , with the continuous attenuation coefficient departing the attenuation coefficient found by clustering at $i\eta \approx 0.25$ for $\bar{k}l_G = 0.9$, and $i\eta \approx 0.18$ for $\bar{k}l_G = 1.1$. This is presumably due to correlation between the modulus of

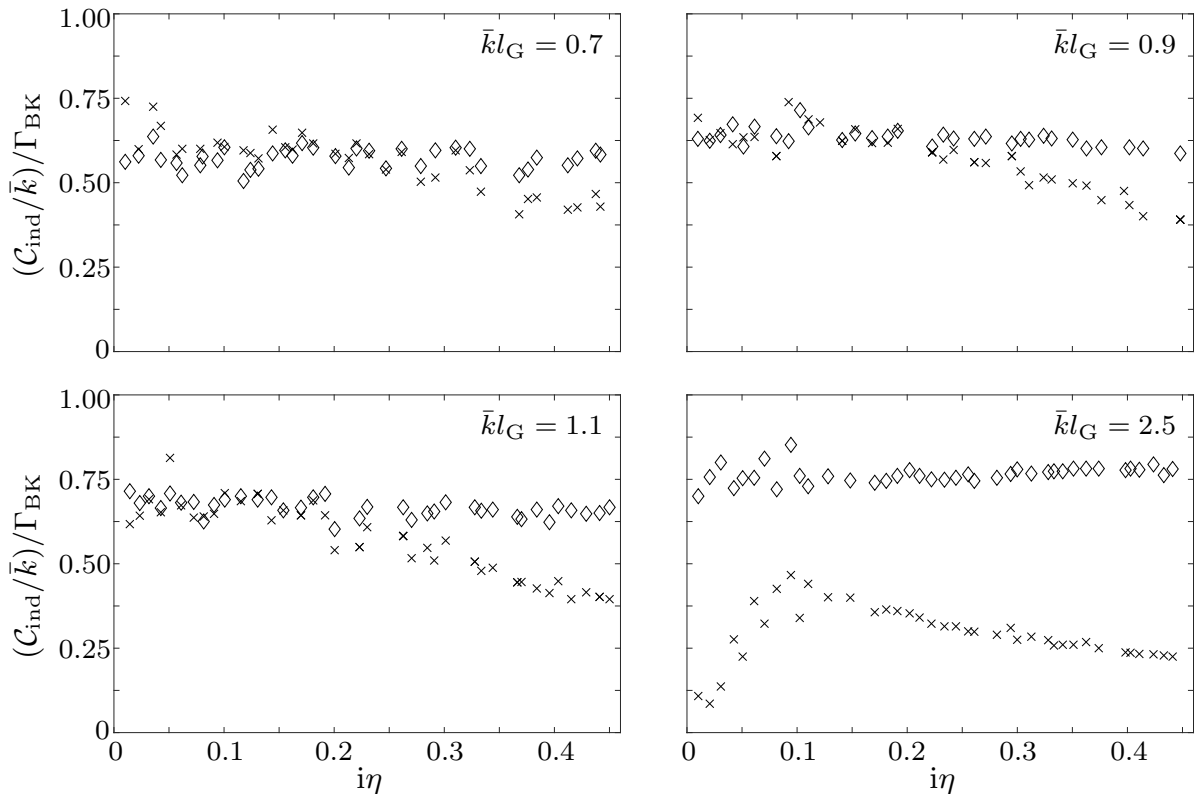


Figure 7: Scaled individual attenuation coefficients for continuous (\times) and clustered (\diamond) problems, as a function of scattering strength, for non-dimensional correlation lengths $\bar{k}l_G = 0.7$ (top left-hand panel), $\bar{k}l_G = 0.9$ (top right), $\bar{k}l_G = 1.1$ (bottom left) and $\bar{k}l_G = 2.5$ (bottom right)

the reflection coefficient and its phase, which becomes more important as the correlation length increases and the phase spreads over a wider range of values, as shown in Fig. 6. For the largest correlation length, $\bar{k}l_G = 2.5$, the continuous attenuation coefficient is significantly smaller than the attenuation coefficient found by clustering for the range of scattering strengths considered, noting that the attenuation rates are very small for large correlation lengths and small scattering strengths, and the increase in the scaled continuous attenuation coefficient for $i\eta < 0.1$ is possibly a numerical artefact associated with difficulties in calculating small attenuation coefficients.

4. Individual vs. effective wave fields

Fig. 7 shows that individual wave fields attenuate at the same rate along a varying string and for its approximating discrete problem formed from the clustering method, over a wide range of parameters. This implies the likely existence of regimes where the individual attenuation coefficients for the varying string can be predicted by the corresponding effective attenuation coefficients (as for the discrete beaded-string problem shown in the right-hand panel of Fig. 1), and, conversely, the individual attenuation coefficients for the beaded-string

problem are significantly less than the corresponding effective attenuations coefficients (as for the continuous problem shown in the left-hand panel of Fig. 1).

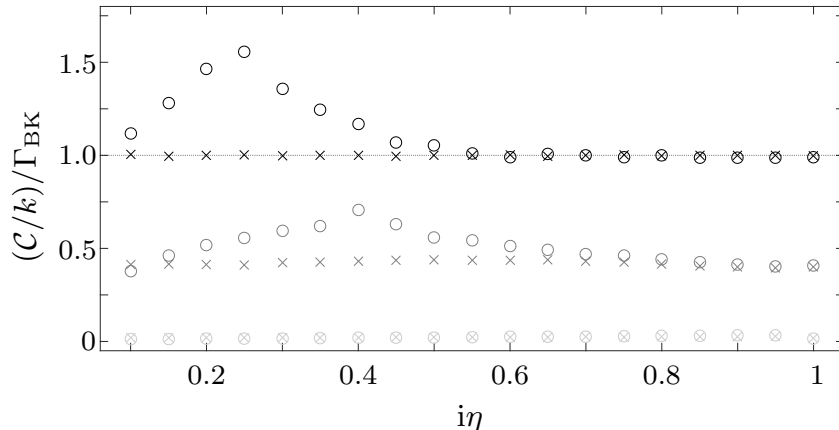


Figure 8: Individual (\times) and effective (\circ) non-dimensional, scaled attenuation coefficients for discrete beaded-string problem, as functions of scattering strength, for values of disorder $\varepsilon k d / \pi = 0.08$ (light grey), $\varepsilon k d / \pi = 0.40$ (dark grey) and $\varepsilon k d / \pi = 1.00$ (black)

Fig. 8 shows (non-dimensional and scaled) individual and effective attenuation coefficients, for the beaded-string problem, as functions of scattering strength, and for positional disorders $\varepsilon k d / \pi = 0.08$, 0.40 and 1.00 . The individual attenuation coefficients are insensitive to the scattering strength in all cases. For the smallest positional disorder, $\varepsilon k d / \pi = 0.08$, the effective attenuation coefficient is indistinguishable from the individual attenuation coefficient. However, for the two larger positional disorders, $\varepsilon k d / \pi = 0.40$ and 1.00 , the effective attenuation coefficients match the individual attenuation coefficients only for large scattering strengths, with the attenuation coefficients matching for $i \eta$ greater than ≈ 0.7 for $\varepsilon k d / \pi = 0.40$, and $i \eta$ greater than ≈ 0.55 for $\varepsilon k d / \pi = 1.00$. For smaller scattering strengths, the effective attenuation coefficients are greater than the individual attenuation coefficients, with the scaled attenuation coefficients being farthest apart at $i \eta = 0.4$ and 0.25 for $\varepsilon k d / \pi = 0.40$ and 1.00 , respectively, and tending towards one another as $i \eta \rightarrow 0$. The deviations for smaller scattering strengths are likely due to wave cancellation effects, which are insignificant for fast attenuating wave fields, i.e. larger scattering strengths. This suggests that a sufficiently large scattering strength is required in order for the effective and individual attenuation coefficients to match, even in the case of discrete scatterers.

Fig. 9 shows log-log plots of individual and effective (non-dimensional and scaled) attenuation coefficients for the varying string problem, as functions of roughness amplitude, for the non-dimensional correlation lengths $\bar{k} l_G = 0.7$ and 2.5 . The scaled attenuation coefficients are insensitive to the roughness amplitude for small roughness amplitudes, specifically $\log_{10} \nu$ less than ≈ -0.8 and ≈ -1.4 for $\bar{k} l_G = 0.7$ and 2.5 , respectively. In these intervals, the scaled effective attenuation coefficient is approximately twice as large as the scaled individual attenuation coefficient for $\bar{k} l_G = 0.7$, i.e. the correlation length at which the individual attenuation rate is near its maximum. For $\bar{k} l_G = 2.5$, i.e. a correlation length for

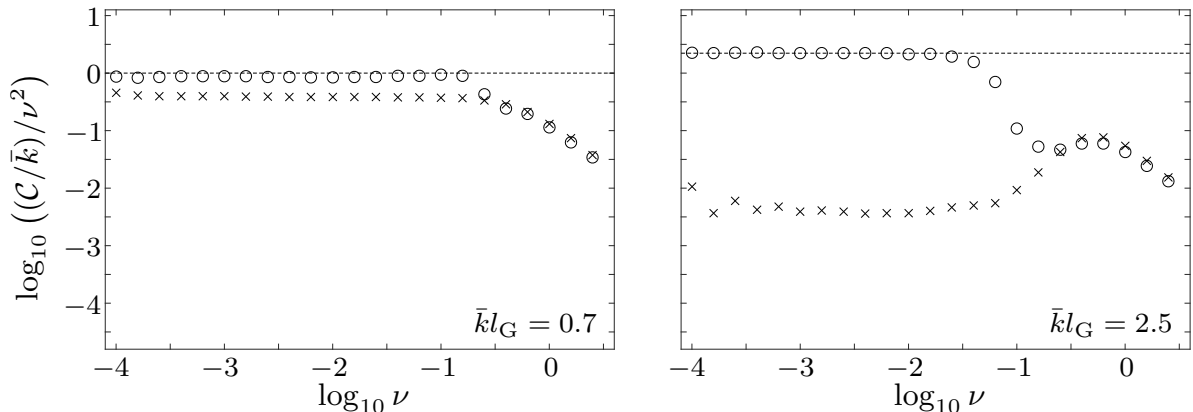


Figure 9: Individual (\times) and effective (\circ) non-dimensional, scaled attenuation coefficients for continuous problem, as functions of roughness amplitude, for non-dimensional correlation length $\bar{k}l_G = 0.7$ (left-hand panel) and $\bar{k}l_G = 2.5$ (right-hand panel)

which the individual wave fields experience negligible attenuation (as shown in the left-hand panel of Fig. 1), the scaled effective attenuation coefficient is larger than the scaled individual attenuation coefficient by approximately three orders of magnitude. For larger roughness amplitudes, the scaled attenuation coefficients vary with the roughness amplitude, with the effective and individual scaled attenuation coefficients monotonically decreasing with increasing roughness amplitude for $\bar{k}l_G = 0.7$, and with more intricate behaviour for $\bar{k}l_G = 2.5$. Strikingly, in the large-roughness-amplitude intervals, the corresponding effective and individual attenuation coefficients rapidly tend towards one another, becoming almost identical for $\log_{10} \nu$ greater than ≈ -0.5 and ≈ -0.6 for $\bar{k}l_G = 0.7$ and 2.5 , respectively, noting that these values can only be reached using the numerical cutoff scheme.

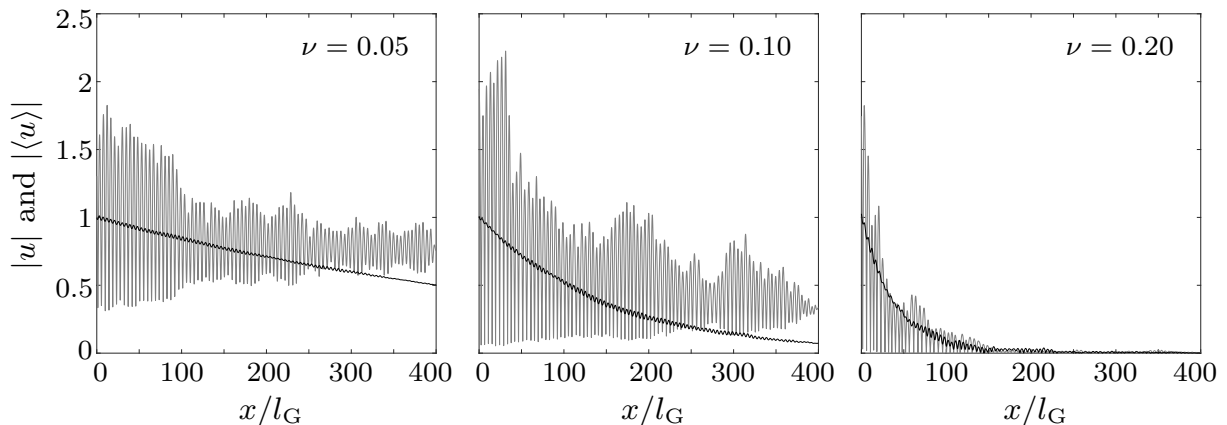


Figure 10: Example individual wave fields (grey curves) and corresponding effective wave fields (black) for continuous problem with non-dimensional correlation length $\bar{k}l_G = 0.7$ and roughness amplitude $\nu = 0.05$ (left-hand panel), $\nu = 0.10$ (middle panel) and $\nu = 0.20$ (right-hand panel)

Fig. 10 shows three example individual wave fields for the continuous problem with

$\bar{k}l_G = 0.7$, and the corresponding effective wave fields. They illustrate the transition in attenuation behaviours as the roughness amplitude increases, as shown in the left-hand panel of Fig. 9. The smallest two roughness amplitudes, $\nu = 0.05$ and 0.10 , are in the interval where the attenuation coefficients are proportional to the roughness amplitude squared, and the effective attenuation coefficient is greater than the individual attenuation coefficient. Stronger attenuation of the effective wave fields than the individual wave fields is evident both for $\nu = 0.05$, where the attenuation rates are relatively slow, and for $\nu = 0.10$, where the attenuation rates are larger, again noting that $\bar{k}l_G = 0.7$ provides the largest attenuation of individual fields. The largest roughness amplitude, $\nu = 0.20$, is just large enough for the effective and individual attenuation coefficients to be close to one another. The wave fields attenuate more rapidly than the wave fields for the smaller roughness amplitudes (noting the scaling of the attenuation coefficients in Fig. 9), and the similarity of the individual and effective attenuation rates is clear, with the effective field approximating the envelope of the individual field.

5. Summary

The investigation was motivated by contrasting previous findings regarding the use of effective wave fields to predict attenuation of individual waves due to random scattering along one-dimensional rough media, with accurate predictions found in discrete scattering problems and inaccurate predictions in continuous problems. Here, a varying string was considered, in which the variations were manifest as continuous random fluctuations in the wavenumber, defined by a Gaussian autocorrelation with specified correlation length and root-mean-square amplitude (roughness amplitude). The varying string can be viewed as a model problem for multiple scattering of waves containing the relevant physics, and the findings potentially also apply to wave propagation in more complicated media and in higher dimensions (in the same scale regime).

For small to mid-range correlation lengths and roughness amplitudes, it was shown that the continuous problem is accurately approximated by a simpler discrete problem, in which scattering characteristics are defined by a single scattering strength (primarily related to the roughness amplitude in the continuous problem) and a kernel function for the phase changes between scatterers (primarily related to the correlation length). This provided evidence of a transition from effective attenuation being unrepresentative of individual attenuation (as in previous investigations for continuous problems) to being representative (as in previous investigations for discrete problems). It was subsequently shown that the scattering strength/roughness amplitude controls the accuracy of the effective attenuation, with, in particular, a sharp transition found in the varying string problem as the roughness amplitude increases, from the effective attenuation being far greater than the individual attenuation to the effective and individual attenuations being almost identical. This key finding required application of a numerical cutoff for non-physical wavenumber values, in order to reach the regime in which the effective attenuation accurately represents the individual attenuation, thus explaining why the transition had not been noted in previous investigations.

Acknowledgement

The authors would like to thank Fabien Montiel for his careful reading of the manuscript. SR acknowledges funding from the Australian government, through an Endeavour Research Fellowship in 2016/2017. LGB and MAP thank the Isaac Newton Institute for Mathematical Sciences for support and hospitality during the programme Mathematics of Sea Ice Phenomena when work on this paper was undertaken, with support by EPSRC (grant number EP/K032208/1). LGB was also partially supported by a grant from the Simons Foundation.

References

- Anderson, P. W., 1958. Absence of diffusion in certain random lattices. *Physical Review* 109 (5), 1492–1505.
- Bennetts, L. G., Peter, M. A., 2013. Spectral analysis of wave propagation through rows of scatterers via random sampling and a coherent potential approximation. *SIAM J. Appl. Math.* 73 (4), 1613–1633.
- Bennetts, L. G., Peter, M. A., Chung, H., 2015. Absence of localisation in ocean wave interactions with a rough seabed in intermediate water depth. *Q. J. Mech. Appl. Math.* 68 (1), 97–113.
- Bennetts, L. G., Squire, V. A., 2009. Wave scattering by multiple rows of circular ice floes. *J. Fluid Mech.* 639, 213–238.
- Berry, M. V., Klein, S., 1997. Transparent mirrors: rays, waves and localization. *Eur. J. Phys.* 18, 222–228.
- Martin, P. A., 2014. N masses on an infinite string and related one-dimensional scattering problems. *Wave Motion* 51, 296–307.
- Maurel, A., Martin, P. A., 2013. Propagation in one-dimensional crystals with positional and compositional disorder. *European Physical Journal B* 86, 486–495.
- Maurel, A., Martin, P. A., Pagneux, V., 2010. Effective propagation in a one-dimensional perturbed periodic structure: comparison of several approaches. *Waves in Random and Complex Media* 20 (4), 634–655.
- Parnell, W. J., Abrahams, I. D., 2008. Multiple scattering in periodic and random media: An overview. Tech. rep., School of Mathematics, University of Manchester (UK).
- Romack, G. M., Weaver, R. L., 1990. Monte carlo studies of multiple scattering of waves in one-dimensional random media. *J. Acoust. Soc. Amer.* 87 (2), 487–494.
- Rupprecht, S., Bennetts, L. G., Peter, M. A., 2017. Effective wave propagation along a rough thin-elastic beam. *Wave Motion* 70, 3–14.
- Sheng, P., 2006. *Introduction to wave scattering, localization and mesoscopic phenomena*. Springer.
- Shinozuka, M., 1971. Simulation of multivariate and multidimensional random processes. *J. Acoust. Soc. Am.* 49 (1), 357–368.
- Silverman, B. W., 1986. *Density Estimation for Statistics and Data Analysis*. Chapman and Hall.
- Wu, R., 1982. Mean field attenuation and amplitude attenuation due to wave scattering. *Wave Motion* 4, 305–316.